

Article

Sulfur Dioxide-Tolerant Core@shell Ru@Pt Catalysts Toward Oxygen Electro-Reduction

Yuxin Liu¹, Changyuan Bao¹, Guodong Xu¹ , Lei Du^{2,*}  and Bing Huang^{1,*}¹ College of Chemical and Environmental Engineering, Yancheng Teachers University, Yancheng 224051, China² Huangpu Hydrogen Innovation Center, School of Chemistry and Chemical Engineering, Guangzhou University, Guangzhou 510006, China

* Correspondence: lei.du@gzhu.edu.cn (L.D.); huangb@yctu.edu.cn (B.H.)

Abstract: Proton exchange membrane fuel cells (PEMFCs) have achieved milestones in performance improvements and commercial launches. In the typical commercialized PEMFCs, the compressed air to cathode is usually supplied from ambient air, assuming that no costly pre-purification system is applied. Therefore, the working PEMFCs may suffer from the negative effects of the air impurities. In this regard, SO₂, as the most poisonous species, may be fed along with air at the cathode and strongly adsorbed on the Pt surface, leading to Pt site deactivation. To address this challenge, we published a series of works in terms of poisoning mechanisms, regeneration protocols, and advanced poisoning-tolerant catalysts. Herein, we are aiming at developing a SO₂-tolerant electrocatalyst toward a cathodic oxygen reduction reaction (ORR). We reasonably incorporate the Ru, synthesize Ru@Pt core@shell catalysts and investigate the relationships among Ru incorporation, ORR activity and SO₂ tolerance. Impressively, the Ru@Pt/C exhibits higher initial ORR activity (0.288 A mg⁻¹_{Pt}), better SO₂ poisoning resistance (33% loss in initial activity) than that of commercial Pt/C catalysts (0.252 A mg⁻¹_{Pt}; 62% loss). The engineered affinity between Pt and SO₂ in the presence of Ru is uncovered to account for the improvement.

Keywords: proton exchange membrane fuel cells; oxygen reduction reaction; sulfur dioxide; poisoning tolerance; core@shell catalysts



Academic Editor: Jae Sung Lee

Received: 19 December 2024

Revised: 23 January 2025

Accepted: 30 January 2025

Published: 3 February 2025

Citation: Liu, Y.; Bao, C.; Xu, G.; Du, L.; Huang, B. Sulfur Dioxide-Tolerant Core@shell Ru@Pt Catalysts Toward Oxygen Electro-Reduction. *Catalysts* **2025**, *15*, 139. <https://doi.org/10.3390/catal15020139>

Copyright: © 2025 by the authors. Licensee MDPI, Basel, Switzerland. This article is an open access article distributed under the terms and conditions of the Creative Commons Attribution (CC BY) license (<https://creativecommons.org/licenses/by/4.0/>).

1. Introduction

Proton exchange membrane fuel cells (PEMFCs) have been considered as an ideal alternative to the traditional internal combustion engine owing to its high energy efficiency and environmental benefits [1–5]. The technological development of PEMFCs has made remarkable progress, and the performance of advanced fuel cell vehicles has been already comparable to the conventional combustion engine vehicles [6–9]. A notable example is the second-generation Toyota Mirai fuel cell, demonstrating an outstanding power density (reaching up to 5.4 kW L⁻¹) [10]. However, there are still significant gaps from the wide deployment of PEMFCs, where the poor stability caused by air impurities is one of the greatest challenges [11–13].

The Pt-based catalyst is sensitive to the poisonous molecules in air such as SO₂ and NO_x, which is ideally supplied directly to cathodes [14,15]. Among others, SO₂ is one of the most poisonous species in ambient air, which strongly adsorbs on the Pt surface and deactivates the active sites [16,17]. It was reported that the loss of PEMFC cell voltage was up to 10% after 20 h of operation in the air containing 0.25 ppm of SO₂ [18]. In addition, SO₂ is hard to remove so that the adsorbed SO₂ could accumulate and gradually increase the SO₂ coverage during fuel cell operation [19,20]. Therefore, the influence of SO₂ is

reasonably significant, and it is urgent to improve the SO₂ tolerance of PEMFCs. At present, fuel cell vehicles usually use air filters to remove air impurities, which are bound in the filter physically or chemically before entering the cathode [21]. However, the adsorption capacity of the filter is limited. It was reported that a fuel cell vehicle needs to be replaced with a new air filter after approximately 10,000 km under normal air quality [22], increasing the application cost. In contrast, exploring innovations in developing advanced SO₂ tolerant catalysts is the fundamental solution to the poor SO₂ tolerance of PEMFC—we have made research in this field in the past years [16,23–25].

To tackle the issue of SO₂ poisoning on the Pt surface, metal oxides and foreign metals were employed and investigated to either accelerate the oxidation of SO_{2ad} or decrease the adsorption energy of SO₂ on Pt surface [26]. For example, CeO₂ [27,28] and TiO₂ [23] have been adopted with the purpose of accelerating the regenerative process. However, decreasing the SO₂ oxidation potential is still challenging: less than 50 mV in negative shift was reported in the literature [23]. In this regard, incorporating the secondary metal with Pt to reduce the activity loss by decreasing the adsorption of SO₂ is promising, such as PtMo [29], Pt₃Co [30,31], and PtRu alloy catalysts [25]. Among them, the SO₂ tolerance of the PtRu alloy catalyst, which was synthesized in our previous work, is the best due to the weaker interaction between Pt and SO₂ [25]. However, the ORR performance of PtRu alloy is poor, due to the abundant ORR-inactive Ru atoms on the surface.

In this work, we incorporate the secondary metal Ru with Pt and synthesize Ru@Pt core@shell catalysts to investigate the relationship among Ru incorporation, ORR activity and SO₂ tolerance. It is inspired that the Ru@Pt/C catalyst not only maintains high ORR activity but also greatly increases the tolerance of SO₂ than commercial Pt/C. The ORR performance and SO₂ tolerance are balanced successfully.

2. Results and Discussion

2.1. Characterization of Catalysts

The Ru@Pt/C core@shell catalysts were prepared using the two-step ethanol reduction method as presented in the experimental section. The actual composition and Pt loading of the Ru@Pt/C is determined by inductively coupled plasma mass spectrometry (ICP-MS). The Pt:Ru molar ratio is 1:1, and the Pt mass loading is 19.83 wt%.

Figure 1a shows the X-ray diffraction (XRD) patterns of the as-prepared Ru@Pt/C catalysts, the peaks at 38.4°, 44.0°, and 69.4° corresponding to (100), (101), and (110) facets of hexagonal Ru (JCPDS No. 89-3942), and the peaks at 40.2°, 46.8° and 68.4° corresponding to (111), (200) and (220) facets of cubic Pt (JCPDS No. 87-0647) [32,33]. As shown in Figure 1a, the diffraction peak of Ru@Pt/C is not offset from the standard diffraction peaks of Pt and Ru, indicating that Pt and Ru are not alloyed [34,35]. Ru and Pt are successfully reduced. The above facts demonstrate that the Ru@Pt/C is synthesized successfully.

Figure 1b shows the transmission electron microscopy (TEM) image of the Ru nanoparticles, and the particles are uniformly loaded on the carbon surface. As shown in Figure 1c, the particle size distributions of the Ru particles are identical with an average diameter of about 3.93 nm. The high resolution TEM (HRTEM) image in Figure 1d shows that the lattice fringe of the obtained nanoparticle is 2.34 Å, corresponding to the (100) lattice plane of Ru, confirming that Ru is successfully anchored on carbon support [36].

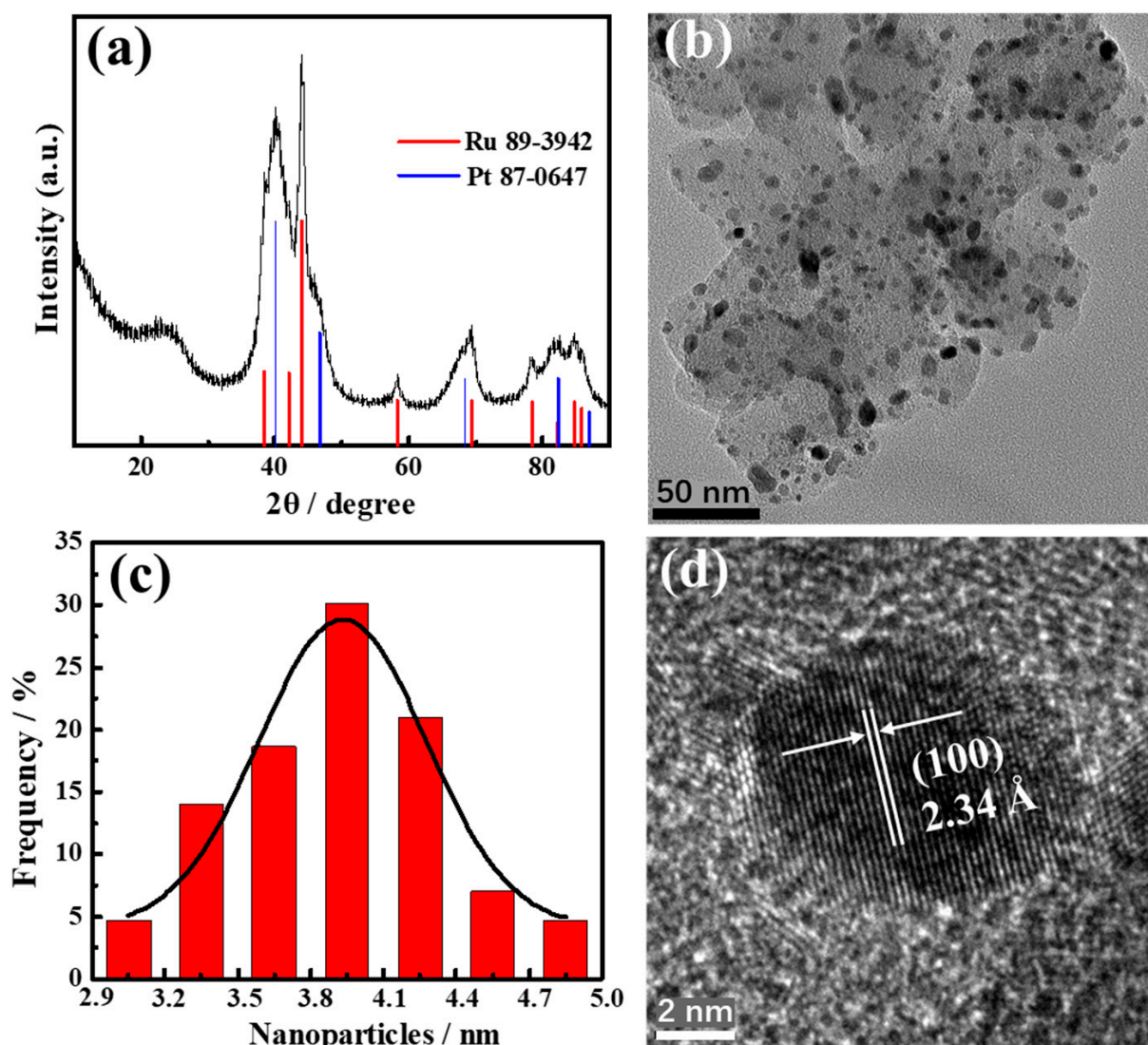


Figure 1. (a) XRD pattern, (b) TEM image, (c) particle size distribution diagram and (d) HRTEM image of Ru/C catalysts.

Figure 2a–c show the TEM images and the corresponding particle size distribution diagram of Ru@Pt/C. It shows that Ru@Pt nanoparticles are uniformly dispersed on the carbon supports with average size of 4.75 nm, which are larger than that of Ru nanoparticles in Figure 1c, suggesting Pt might be deposited on the Ru surface, leading to the formation of Ru@Pt core@shell. The average thickness of the Pt shell is 0.82 nm, which indicates that the Pt shell is about two atoms thick. To ascertain this structure more accurately, the HRTEM image is presented in Figure 2d. It shows that a lattice fringe of 2.34 Å is encircled by another lattice fringe of 2.26 Å, suggesting that Ru oriented in the (100) crystallographic direction is encapsulated by a Pt shell with the (111) surface [37]. Consequently, Ru@Pt/C is successfully synthesized.

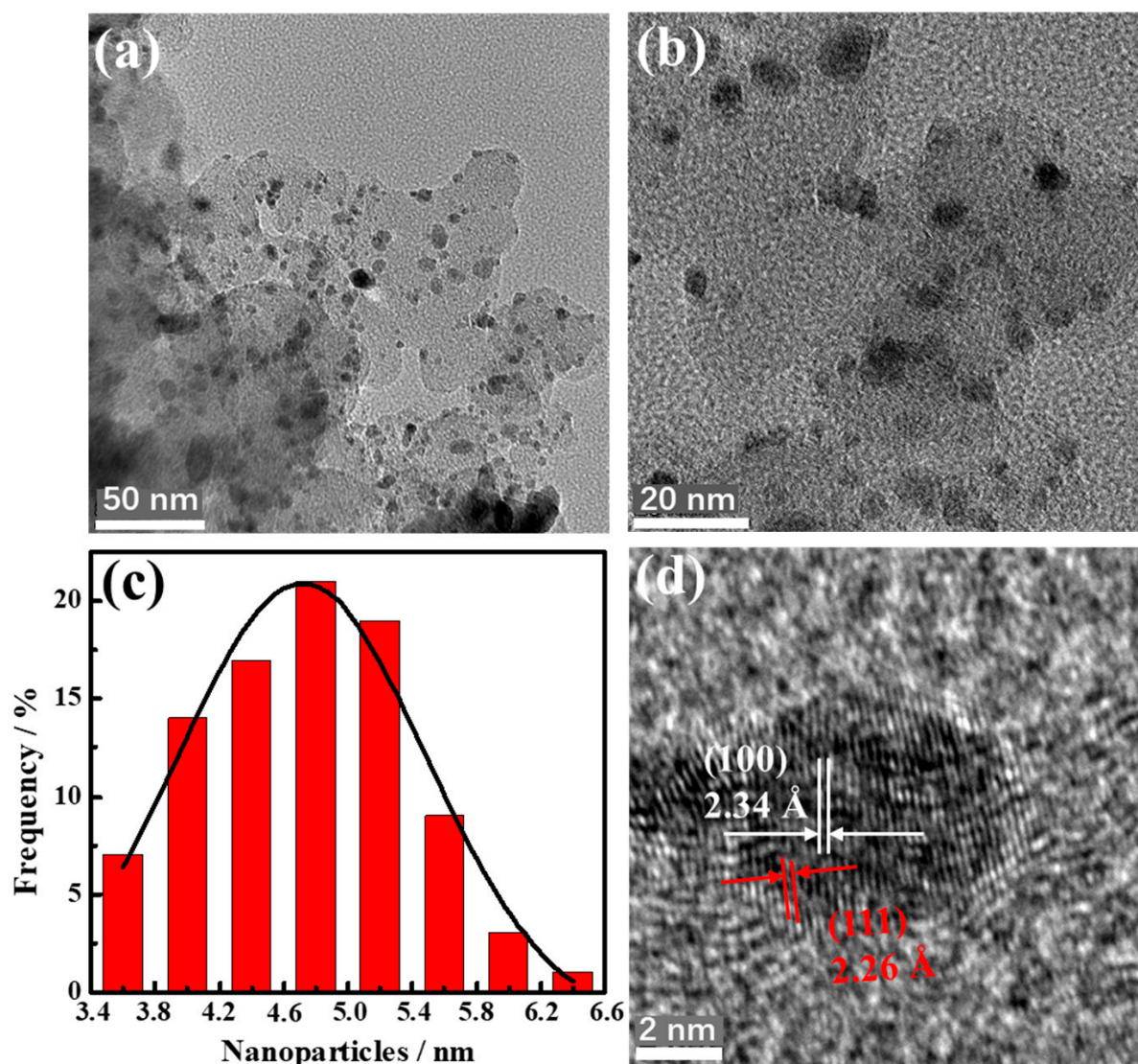


Figure 2. (a,b) TEM images, (c) particle size distribution diagram and (d) HRTEM image of Ru@Pt/C catalysts.

2.2. Electrocatalytic Performance

The cyclic voltammograms (CVs) of Ru/C and Ru@Pt/C in an Ar-saturated 0.1 M HClO₄ solution are shown in Figure 3a. The CV curve of Ru@Pt/C shows the obvious adsorption and desorption current of H on the Pt surface like other published articles show, which is recognized as a characteristic of Pt surface [38,39]. However, the CV curve of Ru/C has no characteristic absorption and desorption current of H, further indicating that Pt has deposited on Ru surface. The Ru@Pt/C catalyst has a core@shell structure with a Pt shell surface [40]. In Figure 3a, the potential of the adsorption peak of oxygen-containing species on the Ru@Pt/C surface is 0.73 V lower than that of Pt/C, which is about 0.85 V, indicating that the OH* functional group is more easily adsorbed on the Ru@Pt/C surface [39].

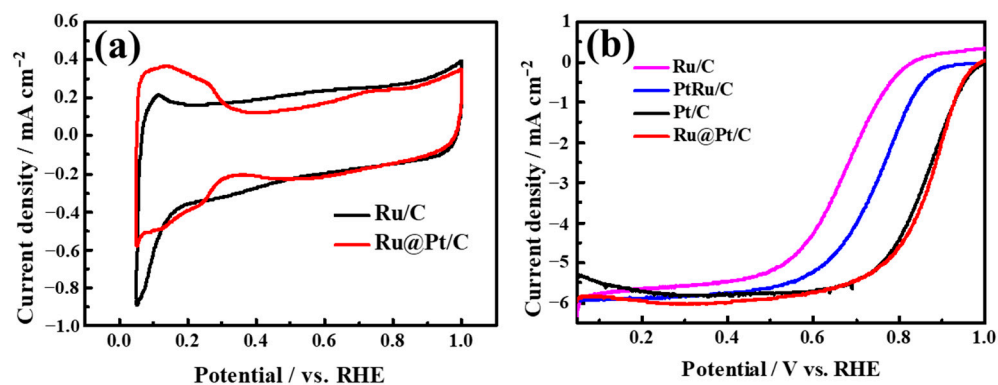


Figure 3. (a) CV curves of Ru/C and Ru@Pt/C; and (b) LSV curves of Ru/C, PtRu/C, commercial Pt/C and Ru@Pt/C.

The ORR performance in an O₂-saturated 0.1 mol·L⁻¹ HClO₄ solution of Ru/C, the commercial Pt/C, Ru@Pt/C and PtRu alloy catalysts (PtRu/C, the Pt:Ru molar ratio and Pt mass loading is similar to Ru@Pt/C) are compared in Figure 3b, and the corresponding electrochemical data of half-wave potential ($E_{1/2}$), mass activity and specific activity at 0.9 V are shown in Table 1. It is not surprising that the ORR activity of Ru/C is the worst, whose $E_{1/2}$ is only 0.670 V, because Ru is inactive for the ORR [41]. The ORR curve of PtRu/C ($E_{1/2}$ = 0.751 V) shifts more positively than Ru/C, indicating that the catalytic activity has been improved after introducing Pt. However, due to the abundant ORR-inactive Ru atoms on the surface, the mass activity (0.015 A mg⁻¹_{Pt}) and specific activity (0.152 mA cm⁻²) at 0.9 V of PtRu/C is less than that of commercial Pt/C catalysts as Table 1 shows. The ORR performance of commercial Pt/C in our work ($E_{1/2}$ = 0.862 V, mass activity at 0.9 V = 0.252 A mg⁻¹_{Pt}, specific activity at 0.9 V = 2.570 mA cm⁻²) is better than other published articles [42,43]. In contrast, the ORR activity of Ru@Pt/C core@shell catalysts is the best, whose $E_{1/2}$, mass activity and specific activity at 0.9 V are 0.872 V, 0.288 A mg⁻¹_{Pt} and 2.983 mA cm⁻² respectively, larger than that of commercial Pt/C, as shown in Figure 3b and Table 1. In short, Ru@Pt core@shell catalysts have the best oxygen reduction performance among Ru/C, commercial Pt/C, Ru@Pt/C and PtRu alloy catalysts, which demonstrates the positive effect of the Ru core to the Pt shell for ORR activity.

Table 1. Electrochemical data of different catalysts in Figure 3b.

Sample	$E_{1/2}$ (V)	Mass Activity (A mg ⁻¹ _{Pt})	Specific Activity (mA cm ⁻²)
Ru/C	0.670	-	-
PtRu/C	0.751	0.015	0.152
Pt/C	0.862	0.252	2.570
Ru@Pt/C	0.872	0.288	2.983

By increasing the high potential limit to 1.2 V, the 1st, 5th, 10th and 20th cycle CV curves for Ru@Pt/C in a fresh Ar-saturated 0.1 M HClO₄ solution at a scan rate of 50 mV s⁻¹ are shown in Figure 4a. With the increase in CV cycles, the double-layer region (0.3–0.5 V) of the CV curve becomes wider, and the characteristics of Ru are gradually obvious. This indicates that the Ru core segregates towards the surface with the increase in scanning potential, resulting in a decrease in Pt shell thickness. The ORR curves of catalysts in Figure 4a are shown in Figure 4b. It is not surprising that the ORR curve shifts negatively with the increase in CV cycles, because of the increasing ORR-inactive Ru atoms on the surface. It indicates that the oxygen reduction performance of Ru@Pt/C improves with the increase in the Pt/Ru atom ratio on surface.

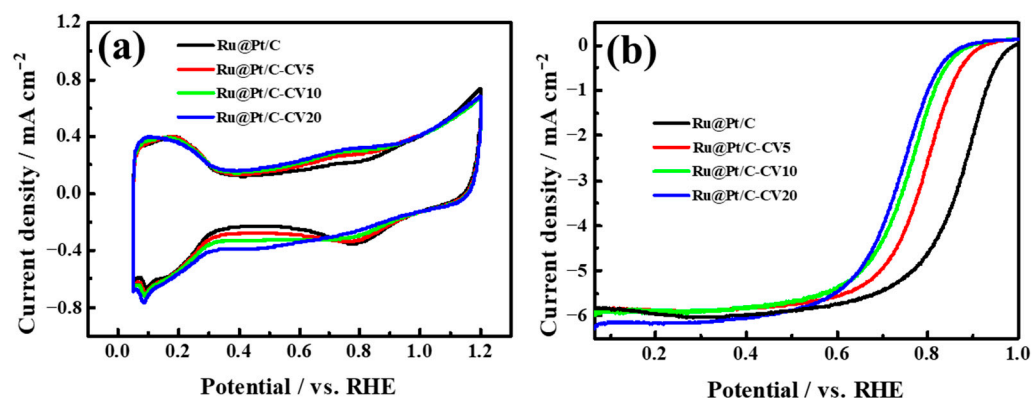


Figure 4. (a) CV curves and (b) LSV curves of Ru@Pt/C after cyclic voltammetry between 0.05 and 1.2 V.

The ORR LSV curves before and after the SO₂ poisoning of Ru@Pt/C and commercial Pt/C are shown in Figure 5a,b. After SO₂ poisoning, the LSV curves of both catalysts shift negatively, indicating that the ORR activity of all catalysts is decreased. However, the SO₂-Ru@Pt/C catalyst still has the best ORR activity compared to SO₂-PtRu/C and SO₂-Pt/C, as shown in Figure 5c, indicating that the SO₂ tolerance of Ru@Pt/C is more advanced. The ORR activities in terms of mass activity at 0.9 V of Ru@Pt/C and commercial Pt/C after SO₂ poisoning are recorded and compared with the initial activity values, as shown in Figure 5d. Obviously, the commercial Pt/C is the most vulnerable to SO₂ poisoning, whose mass activity at 0.9 V decreases from 0.252 A mg⁻¹_{Pt} to 0.096 A mg⁻¹_{Pt} with a loss of 62%. However, the mass activity at 0.9 V of Ru@Pt/C after poisoning decreases from 0.288 A mg⁻¹_{Pt} to 0.192 A mg⁻¹_{Pt}, with only a loss of 33%, which is much less than that of commercial Pt/C. It indicates that the Ru core improves the SO₂ tolerance of the Pt shell.

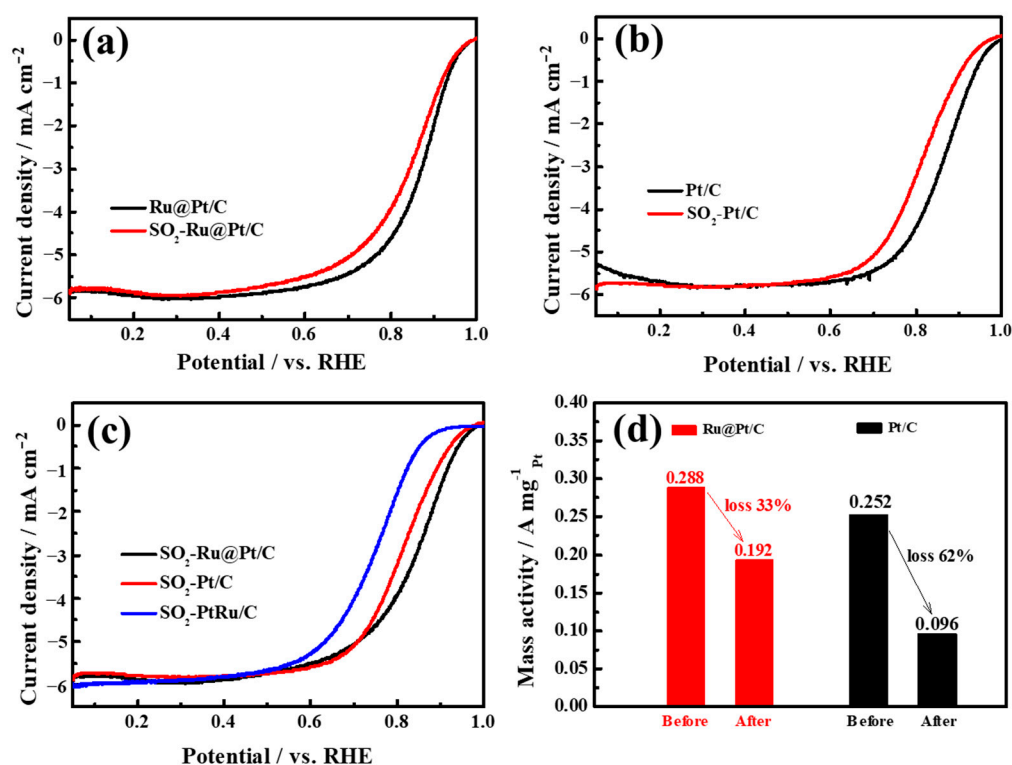


Figure 5. LSV curves of (a) Ru@Pt/C, (b) Pt/C catalysts before and after SO₂ poisoning; (c) LSV curves of SO₂-Ru@Pt/C, SO₂-Pt/C and SO₂-PtRu/C; (d) the mass activity at 0.9 V of Ru@Pt/C and Pt/C catalysts for the ORR before and after SO₂ poisoning.

2.3. Mechanism of SO₂ Tolerance

The X-ray photoelectron spectroscopy (XPS) spectra of elements in the Pt 4f region in Ru@Pt/C and Pt/C are shown in Figure 6. It shows the Pt 4f peak position of Ru@Pt/C XPS spectra shifts positively compared with Pt/C, indicating that the Ru core modifies the electronic structure of Pt. The tuned electronic structure is likely to weaken the SO₂ adsorption of Pt surfaces, which has been confirmed in the reported literature [44]. The decreased SO₂ adsorption is fundamental in enhancing SO₂ tolerance.

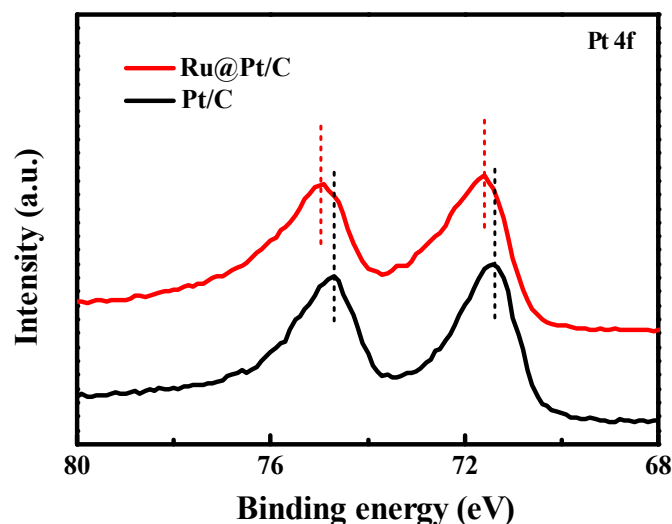


Figure 6. Pt 4f XPS spectra of Ru@Pt/C and Pt/C catalysts.

In order to reveal the effect of Ru on SO₂ tolerance, the theoretical calculation was carried out, which is helpful to understand the adsorption of SO₂ on the model Ru@Pt surface. Figure 7 shows the diagrams of parallel-bonded SO₂ on the model Pt(111) facet and Ru@Pt(111) facet. Silvery and brown big balls represent Pt and Ru atoms, while yellow and red small balls represent S and O atoms, respectively (the ball size does not represent the actual atomic size). According to the study of DFT calculations, the adsorption energies of parallel-bonded SO₂ on Pt(111) and Ru@Pt(111) facets are 1.51 eV and 1.14 eV, respectively. The adsorption energy of SO₂ on Ru@Pt(111) at the parallel site is significantly less than that observed on Pt(111) under the same adsorption configuration. This suggests a weaker interaction between SO₂ and Ru@Pt compared to Pt, facilitating the easier removal of poisonous SO_{2ad} from the Ru@Pt surface.

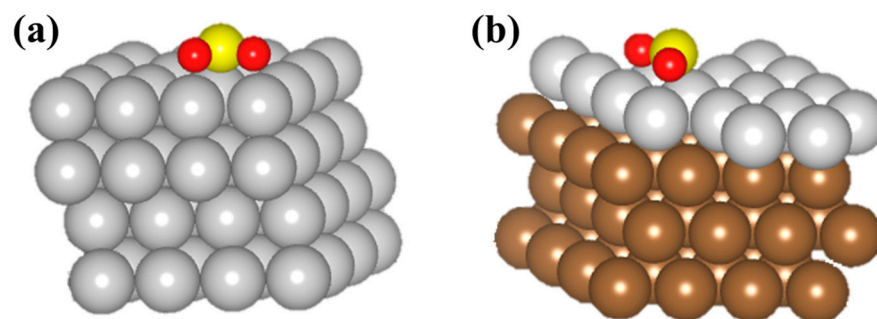


Figure 7. Diagrams of parallel-bonded SO₂ on the model (a) Pt(111) facet and (b) Ru@Pt(111) facet. Silvery and brown big balls represent Pt and Ru atoms, yellow and red small balls represent S and O atoms, respectively.

In summary, compared to the commercial Pt/C catalyst, the Ru@Pt/C demonstrates superior SO₂ tolerance. The Ru core enhances the SO₂ tolerance of Pt shells as illustrated

in Figure 8. The air impurity SO_2 diffuses towards the Ru@Pt/C surface. The Ru core modifies the electronic structure of the Pt shell, weakening the interaction between Pt and SO_2 . Consequently, fewer SO_2 molecules adsorb onto Ru@Pt surfaces, decreasing the loss of ORR activity, boosting the SO_2 tolerance notably.

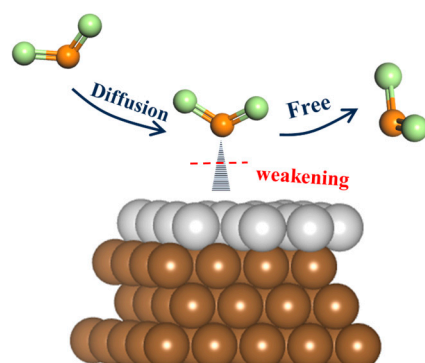


Figure 8. The schematic diagram for the enhanced SO_2 tolerance in Ru@Pt/C catalysts.

3. Materials and Methods

3.1. Chemical and Material Characterization

The commercial Pt/C catalyst (20 wt%, Johnson Matthey Corp, Shanghai, China), Vulcan carbon XC72 (Cabot Corp, Shanghai, China), Chloroplatinic acid (H_2PtCl_6 , Aladdin, Shanghai, China), ethanol ($\text{C}_2\text{H}_5\text{OH}$, Sinopharm Chemical Reagent, Beijing, China), perchloric acid (HClO_4 , Sinopharm Chemical Reagent, Shanghai, China), ruthenium trichloride (RuCl_3 , Aladdin, Shanghai, China), anhydrous sodium sulfite (Na_2SO_3 , Dupont, Shanghai, China), sodium hydroxide (NaOH , Aladdin, Shanghai, China), 5.0 wt% Nafion aqueous solution (Dupont, Wilmington, DE, USA) were purchased and used without further purification. Deionized water (18.2 M Ω cm, Mill-Q Corp, Molsheim, France) was used in all the experiments.

XRD (Panalytical X'PERT) and TEM (FEI Tecnai G2 F30) were used to characterize the morphologies and crystal structure of Ru/C, Ru@Pt/C, Pt/C catalysts. XPS measurements were performed by a Physical Electronics PHI model 5700 instrument using Al K α radiation (1486.6 eV). The binding energy of all samples was calibrated vs. the C1s value of 284.6 eV.

3.2. Synthesis of Catalysts

Synthesis of Ru/C: Firstly, 300 μmol of RuCl_3 was dissolved in 75 mL of ethanol and stirred for 10 min to form a homogeneous solution. Then, the solution was refluxed at 115 $^\circ\text{C}$ with stirring for 1 h in a three-necked flask in order to reduce Ru^{3+} to Ru^{2+} . Meanwhile, 200 mg of Vulcan carbon XC72 was dispersed into 60 mL of ethanol by sonication for 20 min to form a homogeneous suspension liquid. Subsequently, the C suspension was transferred into the reaction flask. After the temperature was stabilized at 110 $^\circ\text{C}$, 9.0 mL of a 0.1 M NaOH solution was injected and continued heating for 2 h. After naturally cooling down, the products were rinsed and dried in a vacuum oven at 60 $^\circ\text{C}$.

Synthesis of Ru@Pt/C: An as-synthesized Ru/C sample was annealed in H_2/N_2 ($V(\text{H}_2): V(\text{N}_2) = 5:95$) at 40 $^\circ\text{C}$ for 2 h and cooled down to room temperature. Then, 100 mg of Ru/C were dissolved in 90 mL of ethanol, and refluxed at 115 $^\circ\text{C}$ for 1 h. After cooling to room temperature, 5 mL of a 30 mM H_2PtCl_6 ethanolic solution was added under vigorously stirring or sonicating to ensure a uniform dispersion. The mixture was heated to 90 $^\circ\text{C}$ and maintained for 2 h. Finally, the solution became colorless; if not, up to 3.0 mL of 0.1 M NaOH was added to completely reduce Pt. After naturally cooling down, the products were rinsed and dried in a vacuum oven at 60 $^\circ\text{C}$.

3.3. Electrochemical Measurements

All electrochemical measurements were performed in a three-electrode system, featuring a Pine AFMSRX disk rotator and an electrochemical workstation (CH Instruments Inc., Bee Cave, TX, USA). A Pt foil served as the counter electrode, while an Ag/AgCl electrode acted as the reference. The catalyst ink was prepared by dispersing 12 mg of the catalyst in a solvent mixture of 9 mL of water, 3 mL of isopropanol, and 12 μL of Nafion (5 wt%) using ultrasonic waves. The working electrode was fabricated by depositing 10 μL of the catalyst ink onto a glassy carbon rotating disk electrode (RDE) with a geometric area of approximately 0.19625 cm^2 .

The electrochemical properties were evaluated using cyclic voltammetry (CV) and linear sweep voltammetry (LSV). Prior to conducting the formal tests, the working electrode was activated through CV scans at a rate of 100 mV s^{-1} within a potential window of 0.05 V to 1 V in an Ar-saturated 0.1 M HClO_4 solution until a stable CV curve was obtained. Subsequently, the oxygen reduction reaction (ORR) activity of the catalysts was assessed using LSV from 0.05 V to 1 V at a scan rate of 10 mV s^{-1} and a rotation speed of 1600 rpm in an O_2 -saturated 0.1 M HClO_4 solution.

The procedure for achieving SO_2 poisoning on Pt surfaces was previously reported in our publication [23,25]. Briefly, the working electrode was poisoned by maintaining it at a potential of 0.65 V in an electrolyte solution containing 0.5 mM of Na_2SO_3 and 0.1 M of HClO_4 for 1 min [23,25]. After poisoning, the electrode was rinsed with water and submerged in a fresh, deoxygenated, and SO_2 -free 0.1 M HClO_4 electrolyte for further electrochemical testing.

All the potentials were reported with respect to the reversible hydrogen electrode (RHE) in this work.

3.4. DFT Calculations

Modeling and theoretical simulations were conducted employing Density Functional Theory (DFT) within a plane-wave pseudopotential framework. A Perdew–Burke–Ernzerhof (PBE) generalized gradient approximate exchange correlation functional was utilized to describe exchange correlation effects in a self-consistent manner. The DFT Semicore pseudopotential approach was adopted for nuclear treatment. Bulk platinum was modeled based on a face-centered cubic lattice structure with a parameter of 3.97 Å. A model of a four-layer-thick 4×4 Pt slab composed of 16 atoms was separated by a vacuum zone of 15 Å. In the case of Ru@Pt(111), the lower three layers of Pt(111) were replaced by Ru(111), and the surface was still the Pt(111) facet. The structural optimization of Pt(111) and Ru@Pt(111) was carried out with medium precision, allowing for full relaxation of the top layer atoms and adsorbates, while the bottom three layers were constrained to their bulk positions. The adsorption energy of SO_2 was calculated following the below equation [25]:

$$E_{ads} = -\left(E_{\text{SO}_2-M(111)} - E_{M(111)} - E_{\text{SO}_2}\right)$$

where $E_{\text{SO}_2-M(111)}$ represents the energy of the SO_2 molecule adsorbed on the metal (111) surface, $E_{M(111)}$ represents the energy of the bare metal (111) surface, and E_{SO_2} represents the energy of the SO_2 molecule in its gaseous state.

4. Conclusions

In conclusion, Ru@Pt/C core@shell catalysts have been designed and synthesized to investigate the relationship among Ru incorporation, ORR activity and SO_2 tolerance. The Ru@Pt/C exhibits a higher catalytic activity and better SO_2 poisoning resistance than the commercial Pt/C. The ORR mass activity of Ru@Pt/C catalyst is 0.288 $\text{A mg}^{-1}_{\text{Pt}}$ higher

than that of commercial Pt/C ($0.252 \text{ A mg}^{-1}_{\text{Pt}}$). In addition, the ORR mass activity of Ru@Pt/C only lost 33% after SO_2 poisoning, which is much better than the SO_2 tolerance of commercial Pt/C that lost 62% of mass activity under the same poisoning condition. Physical characterization and theoretical calculation demonstrate that the Ru core efficiently modifies the electronic structure of Pt shell and leads to weaker interaction between Pt and SO_2 . This work balances the ORR performance and SO_2 tolerance successfully.

Author Contributions: Synthesis and characterization, Y.L.; electrocatalytic experiments, Y.L. and C.B.; supervision, L.D. and B.H.; project administration, Y.L. and L.D.; writing, Y.L. and L.D.; proof-read, G.X. All authors have read and agreed to the published version of the manuscript.

Funding: This research was funded by the Natural Science Foundation of Jiangsu Province (BK20230720), the Natural Science Foundation of the Jiangsu Higher Education Institutions of China (23KJB530013), the Basic and Applied Basic Research Foundation of Guangdong Province (2022B1515120079), and the Natural Science Foundation of Guangdong Province (2022B1515020020).

Data Availability Statement: Data are available in the main text.

Conflicts of Interest: The authors declare no conflicts of interest.

References

1. Wei, X.; Chan, K.W.; Wu, T.; Wang, G.; Zhang, X.; Liu, J. Wasserstein distance-based expansion planning for integrated energy system considering hydrogen fuel cell vehicles. *Energy* **2023**, *272*, 127011. [[CrossRef](#)]
2. Bao, C.; Jiang, Y.; Zhong, H.; Ren, H.; Wang, J.; Liu, B.; Zhao, Q.; Jin, F.; Chong, Y.M.; Sun, J. Synergizing 3D-printed structure and sodiophilic interface enables highly efficient sodium metal anodes. *Chin. Chem. Lett.* **2024**, *35*, 109353. [[CrossRef](#)]
3. Snitkoff-Sol, R.Z.; Rimon, O.; Bond, A.M.; Elbaz, L. Direct measurement of the oxygen reduction reaction kinetics on iron phthalocyanine using advanced transient voltammetry. *Nat. Catal.* **2024**, *7*, 139–147. [[CrossRef](#)]
4. Wang, J.; Pan, F.; Chen, W.; Li, B.; Yang, D.; Ming, P.; Wei, X.; Zhang, C. Pt-based intermetallic compound catalysts for the oxygen reduction reaction: Structural control at the atomic scale to achieve a win–win situation between catalytic activity and stability. *Electrochem. Energy Rev.* **2023**, *6*, 6. [[CrossRef](#)]
5. Alenazey, F.; Alyousef, Y.; AlOtaibi, B.; Almutairi, G.; Minakshi, M.; Cheng, C.K.; Vo, D.-V.N. Degradation behaviors of solid oxide fuel cell stacks in steady-state and cycling conditions. *Energy Fuels* **2020**, *34*, 14864–14873. [[CrossRef](#)]
6. Zhao, S.L.; Yang, Y.C.; Tang, Z.Y. Insight into structural evolution, active sites, and stability of heterogeneous electrocatalysts. *Angew. Chem. Int. Ed.* **2022**, *61*, e202110186. [[CrossRef](#)] [[PubMed](#)]
7. Zhao, W.; Xu, G.; Dong, W.; Zhang, Y.; Zhao, Z.; Qiu, L.; Dong, J. Progress and perspective for in situ studies of oxygen reduction reaction in proton exchange membrane fuel cells. *Adv. Sci.* **2023**, *10*, 2300550. [[CrossRef](#)]
8. Pramuanjaroenkij, A.; Kakaç, S. The fuel cell electric vehicles: The highlight review. *Int. J. Hydrogen Energy* **2023**, *48*, 9401–9425. [[CrossRef](#)]
9. Xu, J.; Zhang, C.; Wan, Z.; Chen, X.; Chan, S.H.; Tu, Z. Progress and perspectives of integrated thermal management systems in PEM fuel cell vehicles: A review. *Renew. Sust. Energy Rev.* **2022**, *155*, 111908. [[CrossRef](#)]
10. Chen, Y.; Huang, Z.Y.; Yu, J.F.; Wang, H.Y.; Qin, Y.K.; Xing, L.X.; Du, L. Research Progress of Pt-Based Catalysts toward Cathodic Oxygen Reduction Reactions for Proton Exchange Membrane Fuel Cells. *Catalysts* **2024**, *14*, 569. [[CrossRef](#)]
11. Miao, C.; Yu, S.; Zhang, Y.; Hu, Y.; He, X.; Chen, W. Assessing outdoor air quality vertically in an urban street canyon and its response to microclimatic factors. *J. Environ. Sci.* **2023**, *124*, 923–932. [[CrossRef](#)] [[PubMed](#)]
12. Matsui, H.; Sato, K.; Isobe, N.; Samjeské, G.; Uruga, T.; Tada, M. Spatial imaging of catalyst poisoning with SO_2 on Pt/C PEFC electrocatalyst by operando Pt L III-edge XAFS-CT imaging. *Catal. Sci. Technol.* **2023**, *13*, 4360–4366. [[CrossRef](#)]
13. Kuo, J.-K.; Thamma, U.; Wongcharoen, A.; Chang, Y.-K. Optimized fuzzy proportional integral controller for improving output power stability of active hydrogen recovery 10-kW PEM fuel cell system. *Int. J. Hydrogen Energy* **2024**, *50*, 1080–1093. [[CrossRef](#)]
14. Main, R.M.; Vornholt, S.M.; Ettlinger, R.; Netzsch, P.; Stanzione, M.G.; Rice, C.M.; Elliott, C.; Russell, S.E.; Warren, M.R.; Ashbrook, S.E. In Situ single-crystal X-ray diffraction studies of physisorption and chemisorption of SO_2 within a metal–organic framework and its competitive adsorption with water. *J. Am. Chem. Soc.* **2024**, *146*, 3270–3278. [[CrossRef](#)] [[PubMed](#)]
15. Baturina, O.A.; Gould, B.D.; Korovina, A.; Garsany, Y.; Stroman, R.; Northrup, P.A. Products of SO_2 adsorption on fuel cell electrocatalysts by combination of sulfur K-edge XANES and electrochemistry. *Langmuir* **2011**, *27*, 14930–14939. [[CrossRef](#)]
16. Liu, Y.-X.; Zhang, W.-Y.; Han, G.-K.; Zhou, Y.-W.; Li, L.-F.; Kang, C.; Kong, F.-P.; Gao, Y.-Z.; Du, C.-Y.; Wang, J.-J. Deactivation and regeneration of a benchmark Pt/C catalyst toward oxygen reduction reaction in the presence of poisonous SO_2 and NO. *Catal. Sci. Technol.* **2022**, *12*, 2929–2934. [[CrossRef](#)]

17. Awad, M.; Saleh, M.; Ohsaka, T. Impact of SO₂ poisoning of platinum nanoparticles modified glassy carbon electrode on oxygen reduction. *J. Power Sources* **2011**, *196*, 3722–3728. [[CrossRef](#)]
18. Reshetenko, T.; Laue, V.; Krewer, U.; Artyushkova, K. Study of degradation and spatial performance of low Pt-loaded proton exchange membrane fuel cells under exposure to sulfur dioxide in an oxidant stream. *J. Power Sources* **2020**, *458*, 228032. [[CrossRef](#)]
19. Punyawudho, K.; Ma, S.; Van Zee, J.; Monnier, J. Effect of O₂ on the adsorption of SO₂ on carbon-supported Pt electrocatalysts. *Langmuir* **2011**, *27*, 7524–7530. [[CrossRef](#)]
20. Dourado, A.H.; Munhos, R.L.; Silva Jr, N.A.; Colle, V.D.; Carvalho, G.G.; Oliveira, P.V.; Arenz, M.; Varela, H.; Cordoba de Torresi, S.I. Opportunities and knowledge gaps of SO₂ electrocatalytic oxidation for H₂ electrochemical generation. *ACS Catal.* **2019**, *9*, 8136–8143. [[CrossRef](#)]
21. Tang, M.H.; Zhang, S.M.; Chen, S.L. Pt utilization in proton exchange membrane fuel cells: Structure impacting factors and mechanistic insights. *Chem. Soc. Rev.* **2022**, *51*, 1529–1546. [[CrossRef](#)] [[PubMed](#)]
22. Xu, N.; Zhang, Y.; Fu, Z.; Zhao, D.; Chu, L.; Zhou, F. Investigation of Topologies and Control Strategies of Fuel Cell Vehicles. In Proceedings of the International Conference on Advances in Mechanical Engineering and Industrial Informatics (AMEII), Zhengzhou, China, 11–12 April 2015; pp. 1651–1654.
23. Liu, Y.; Ye, J.; Kong, F.; Du, C.; Zuo, P.; Du, L.; Yin, G. Pt/C-TiO₂ as oxygen reduction electrocatalysts against sulfur poisoning. *Catalysts* **2022**, *12*, 571. [[CrossRef](#)]
24. Liu, Y.-X.; Zhang, W.-Y.; Han, G.-K.; Zhou, Y.-W.; Li, L.-F.; Kong, F.-P.; Gao, Y.-Z.; Du, C.-Y.; Wang, J.-J.; Du, L. Deactivated Pt electrocatalysts for the oxygen reduction reaction: The regeneration mechanism and a regenerative protocol. *ACS Catal.* **2021**, *11*, 9293–9299. [[CrossRef](#)]
25. Liu, Y.; Du, L.; Kong, F.; Han, G.; Gao, Y.; Du, C.; Zuo, P.; Yin, G. Sulfur dioxide-tolerant bimetallic PtRu catalyst toward oxygen electroreduction. *ACS Sustain. Chem. Eng.* **2019**, *8*, 1295–1301. [[CrossRef](#)]
26. Zhao, Z.; Liu, Z.; Zhang, A.; Yan, X.; Xue, W.; Peng, B.; Xin, H.L.; Pan, X.; Duan, X.; Huang, Y. Graphene-nanopocket-encaged PtCo nanocatalysts for highly durable fuel cell operation under demanding ultralow-Pt-loading conditions. *Nat. Nanotechnol.* **2022**, *17*, 968–975. [[CrossRef](#)] [[PubMed](#)]
27. Xu, F.; Cheng, K.; Yu, Y.; Mu, S. One-pot synthesis of Pt/CeO₂/C catalyst for enhancing the SO₂ electrooxidation. *Electrochim. Acta* **2017**, *229*, 253–260. [[CrossRef](#)]
28. Xu, F.; Xu, R.; Mu, S. Enhanced SO₂ and CO poisoning resistance of CeO₂ modified Pt/C catalysts applied in PEM fuel cells. *Electrochim. Acta* **2013**, *112*, 304–309. [[CrossRef](#)]
29. Xia, M.; Liu, Y.; Li, L.; Xiong, K.; Qi, X.; Yang, L.; Hu, B.; Xue, Y.; Wei, Z. A DFT study on PtMo resistance to SO₂ poisoning. *Sci. China Chem.* **2013**, *56*, 1004–1008. [[CrossRef](#)]
30. Pillay, D.; Johannes, M.; Garsany, Y.; Swider-Lyons, K. Poisoning of Pt₃Co electrodes: A combined experimental and DFT study. *J. Phys. Chem. C* **2010**, *114*, 7822–7830. [[CrossRef](#)]
31. Garsany, Y.; Baturina, O.A.; Swider-Lyons, K.E. Oxygen reduction reaction kinetics of SO₂-contaminated Pt₃Co and Pt/Vulcan carbon electrocatalysts. *J. Electrochem. Soc.* **2009**, *156*, B848. [[CrossRef](#)]
32. You, S.-H.; Lee, W.; Jang, H.Y.; Kim, K.-S.; Baek, J.; Choe, G.; Ji, S.G.; Paidi, V.K.; Choi, C.H.; Back, S. Optimizing the Atomic Structure of Ruthenium Deposited on Pt/C Cathode Catalysts to Enhance Durability of Automotive Fuel Cell. *Appl. Catal. B Environ.* **2024**, *359*, 124486. [[CrossRef](#)]
33. Zhong, H.-L.; Ze, H.; Zhang, X.-G.; Zhang, H.; Dong, J.-C.; Shen, T.; Zhang, Y.-J.; Sun, J.-J.; Li, J.-F. In situ SERS probing the effect of additional metals on Pt-based ternary alloys toward improving ORR performance. *ACS Catal.* **2023**, *13*, 6781–6786. [[CrossRef](#)]
34. Berova, V.; Manjón, A.G.; Paredes, M.V.; Schwarz, T.; Rivas, N.A.; Hengge, K.; Jurzinsky, T.; Scheu, C. Influence of the shell thickness on the degradation of Ru@Pt core-shell catalysts in PEM fuel cells. *J. Power Sources* **2023**, *554*, 232327. [[CrossRef](#)]
35. Yang, J.; Feng, J.; Cao, Y.; Xiao, Y.; Qiao, L.; An, K.; Yang, J.; Peng, J.; Pan, H.; Cheng, H.M. Highly dispersed Ru-Pt heterogeneous nanoparticles on reduced graphene oxide for efficient pH-universal hydrogen evolution. *Adv. Funct. Mater.* **2024**, *34*, 2411081. [[CrossRef](#)]
36. Wang, Y.; Wang, J.; Han, G.; Du, C.; Sun, Y.; Du, L.; An, M.; Yin, G.; Gao, Y.; Song, Y. Superior catalytic performance and CO tolerance of Ru@Pt/C-TiO₂ electrocatalyst toward methanol oxidation reaction. *Appl. Surf. Sci.* **2019**, *473*, 943–950. [[CrossRef](#)]
37. Yang, F.; Wang, Y.; Cui, Y.; Yang, X.; Zhu, Y.; Weiss, C.M.; Li, M.; Chen, G.; Yan, Y.; Gu, M.D. Sub-3 nm Pt@Ru toward outstanding hydrogen oxidation reaction performance in alkaline media. *J. Am. Chem. Soc.* **2023**, *145*, 27500–27511. [[CrossRef](#)]
38. Liu, X.; Wang, Y.; Liang, J.; Li, S.; Zhang, S.; Su, D.; Cai, Z.; Huang, Y.; Elbaz, L.; Li, Q. Introducing electron buffers into intermetallic Pt alloys against surface polarization for high-performing fuel cells. *J. Am. Chem. Soc.* **2024**, *146*, 2033–2042. [[CrossRef](#)]
39. Hoshi, N.; Nakamura, M.; Kubo, R.; Suzuki, R. Enhanced oxygen reduction reaction on caffeine-modified platinum single-crystal electrodes. *Commun. Chem.* **2024**, *7*, 23. [[CrossRef](#)] [[PubMed](#)]
40. Zhang, J.; Wang, M.; Wan, T.; Shi, H.; Lv, A.; Xiao, W.; Jiao, S. Novel (Pt-Ox)-(Co-Oy) nonbonding active structures on defective carbon from oxygen-rich coal tar pitch for efficient HER and ORR. *Adv. Mater.* **2022**, *34*, 2206960. [[CrossRef](#)] [[PubMed](#)]

41. Cao, X.; Huo, J.; Li, L.; Qu, J.; Zhao, Y.; Chen, W.; Liu, C.; Liu, H.; Wang, G. Recent advances in engineered Ru-based electrocatalysts for the hydrogen/oxygen conversion reactions. *Adv. Energy Mater.* **2022**, *12*, 2202119. [[CrossRef](#)]
42. Wei, X.; Song, S.; Cai, W.; Kang, Y.; Fang, Q.; Ling, L.; Zhao, Y.; Wu, Z.; Song, X.; Xu, X.; et al. Pt Nanoparticle-Mn single-atom pairs for enhanced oxygen reduction. *ACS Nano* **2024**, *18*, 4308–4319. [[CrossRef](#)] [[PubMed](#)]
43. Lv, H.; Zheng, Y.; Wang, Y.; Wang, J.; Liu, B.; Qiao, Z.-A. Ordered Mesoporous Intermetallic Ga-Pt nanoparticles: Phase-controlled synthesis and performance in oxygen reduction electrocatalysis. *Angew. Chem. Int. Ed.* **2023**, *62*, e202304420. [[CrossRef](#)] [[PubMed](#)]
44. Ni, W.; Meibom, J.L.; Hassan, N.U.; Chang, M.; Chu, Y.-C.; Krammer, A.; Sun, S.; Zheng, Y.; Bai, L.; Ma, W. Synergistic interactions between PtRu catalyst and nitrogen-doped carbon support boost hydrogen oxidation. *Nat. Catal.* **2023**, *6*, 773–783. [[CrossRef](#)]

Disclaimer/Publisher's Note: The statements, opinions and data contained in all publications are solely those of the individual author(s) and contributor(s) and not of MDPI and/or the editor(s). MDPI and/or the editor(s) disclaim responsibility for any injury to people or property resulting from any ideas, methods, instructions or products referred to in the content.